Exploration of mechanisms of drug resistance by polyaneuploid cancer cells in a microfluidic device and patient tissues

Wanyoung Lim[1]†, Inwoo Hwang[2]†, Jiande Zhang[3], Zhenzhong Chen[3], Jeonghun Han[3], Bon-Kyoung Koo[4], Sangmin Kim[5], Jeong Eon Lee[6], Kenneth J. Pienta[7], Sarah R. Amend[7], Robert H. Austin[8], Jee-Yin Ahn[2,9,10]*, and Sungsu Park[1,3,11]*

[1]*Department of Biomedical Engineering, Sungkyunkwan University, Suwon 16419, South Korea*
[2]*Department of Molecular Cell Biology, Sungkyunkwan University School of Medicine, Suwon 16419, South Korea*
[3]*School of Mechanical Engineering, Sungkyunkwan University, Suwon 16419, South Korea*
[4]*Institute of Molecular Biotechnology of the Austrian Academy of Sciences (IMBA), Vienna Biocenter (VBC), 1030 Vienna, Austria*
[5]*Department of Breast Cancer Center, Samsung Medical Center, Sungkyunkwan University School of Medicine, Seoul 06351, South Korea*
[6]*Division of Breast Surgery, Department of Surgery, Samsung Medical Center, Sungkyunkwan University School of Medicine, Seoul 06351, South Korea*
[7]*The Cancer Ecology Center at the James Buchanan Brady Urological Institute, Johns Hopkins School of Medicine, Baltimore, MD 21205, USA*
[8]*Department of Physics, Princeton University, Princeton, NJ 08544, USA*
[9]*Single Cell Network Research Center, Sungkyunkwan University School of Medicine, Suwon 16419, South Korea*
[10]*Samsung Biomedical Research Institute, Samsung Medical Center, Sungkyunkwan University School of Medicine, Seoul 06351, South Korea*
[11]*Institute of Quantum Biophysics (IQB), Sungkyunkwan University, Suwon 16419, South Korea*

*Corresponding authors. E-mail: jeeahn@skku.edu; nanopark@skku.edu

†These authors contributed equally to this work.

Abstract

Chemoresistance can be increased by cells in the polyaneuploid cancer cells (PACC) state, a major cause of treatment failure in various cancers. The life cycle of cells in the PACC state is understudied, and the mechanism of their drug resistance is unknown. In this study, we induced the development of doxorubicin (DOX)-resistant PACCs from triple negative breast cancer (TNBC) cells within 11 days using a microfluidic device that generates a DOX concentration gradient. In vivo chemoresistant xenograft models, an unbiased genome-wide transcriptome analysis, and a patient data/tissue analysis all showed that chemoresistance of the PACCs arose from failed epigenetic control of the nuclear protein-1 (NUPR1)/histone deacetylase 11 (HDAC11) axis, and high Nupr1 expression correlated with poor clinical outcomes. These results suggest that the chip can rapidly induce clinically relevant PACCs, and that cells in the PACC state increase tumor heterogeneity and chemoresistance.

Teaser

Drug resistance of polyaneuploid cancer cells in a microfluidic device and patient tissues.

Keywords: Polyaneuploid cancer cells (PACCs), microfluidic device, nuclear protein-1 (NUPR1), histone deacetylase 11 (HDAC11)

Introduction

A leading cause of cancer-related death is drug resistance (*1*), which is increased by tumor heterogeneity(*2*). One form of tumor heterogeneity that has been associated with increased drug resistance is the polyaneuploid cancer cell (PACC) state (*3, 4*). Cells in the PACC state (PACCs) have been described by many names including polyploid giant cancer cells (PGCCs) and are present in multiple high-grade and post-treatment cancers (*3, 4*). Various environmental factors, including hypoxia (*4*), anticancer drugs (*5-7*), and radiation therapy (*8*), cause recurrent mitotic/mitotic failure or genomic instability in cancer cells, which leads to PACC formation (*5*). For example, paclitaxel-treated ovarian cancer cells with defects in cell division and mitotic spindle assembly can form PACCs (*5, 9*). Cells in the PACC state self-renew and have been demonstrated to have the capacity to further divide into small daughter cells by nuclear budding or asymmetric division (*10*), contributing to an increase in tumor heterogeneity. The life cycle of the PACC state is relatively well understood but the mechanism by which PACCs confer drug resistance is unknown. Elucidating the underlying mechanisms by which cancer cells transform into chemoresistant PACCs will open new ways to overcome drug resistance.

Nuclear protein-1 (NUPR1; also known as Com-1 or p8) is involved in multiple aspects of cancer, including DNA repair, transcription regulation, and the cell cycle, and its expression responds to stress signals induced by genotoxic signals and agents (*11*). Nupr1 influences cancer cell resistance (*12*) and promotes the proliferation of cancer cells bypassing the G0/G1 check point (*13*). In breast cancer cells, NUPR1 upregulates p21 transcription, allowing breast cancer cells to progress through the cell cycle, and it confers resistance to chemotherapeutic agents such as taxol and doxorubicin (DOX) (*14, 15*). Increased expression of NUPR1 has previously been associated with poor patient outcomes in certain types of cancers (*16, 17*).

Histone deacetylase 11 (HDAC11) is the most recently discovered member of the HDAC family and the only member of class IV. It displays different expression levels and biological functions in different human organs and systems. Its overexpression in various cancers, including hepatocellular, ovarian, myeloma, lymphoma, and breast cancers (*18-22*), has suggested HDAC11 is an epigenetic regulator in human cancers. However, HDAC11 expression is negatively correlated with high-risk uveal melanomas and gliomas (*23*), and HDAC11 knockout mice demonstrate increased tumor growth (*24*), indicating that its regulation of different cancer types is complex. Therefore, the pathophysiological roles of HDAC11 in various cancers should be evaluated.

Microfluidic chips are highly useful for studying drug resistance because they can manipulate and control fluids and particles at the micron level (*25*). Recently, a microfluidic platform consisting of an array of connected microchambers with concentration gradients has

been developed to induce drug resistance in various types of cancers, such as triple negative breast cancer (TNBC) (*26, 27*), glioblastoma (GBM) (*28*), and prostate cancer (*29*). We previously identified the molecular mechanisms involved in drug resistance in GBM and TNBC by analyzing mutation and expression data from chemoresistant cancer cells (*27, 28*). Recently, Lin *et al*. used a microfluidic chip that generates a docetaxel gradient to induce cells in the PACC state from PC-3 prostate cancer cells (*29*). However, the underlying mechanisms by which PACCs acquire chemoresistance and whether PACCs obtained from a chip resemble those found in patient tissues remain unknown.

In this study, we induced DOX-resistant PACCs from MDA-MB-231 TNBC cells within 11 days using the Cancer Drug Resistance Accelerator (CDRA) chip (*28*) generating gradients of DOX and medium. DOX-resistant PACCs PACCs were isolated using fluorescence-activated cell sorting (FACS), and we combined *in vivo* chemoresistant xenograft models with an unbiased genome-wide transcriptome analysis and patient data/tissue analysis to identify the mechanisms of PACCs chemoresistance in TNBC. We demonstrate that the chemoresistance of PACCs arises from failed epigenetic control of the NUPR1/HDAC11 axis and is reduced by Nupr1 inhibition (Fig. 1).

Results

Formation and characterization of PGCCs

Approximately 30 wild type (WT) MDA-MB-231 cells per microchamber were seeded through the cell seeding hole in the CDRA chip (Fig. 2a–c). The day after seeding, the cells were perfused with gradients of medium and DOX (1.5 μM) (Fig. 2a, b, e). Cells exposed to a high concentration of DOX (high-DOX region) were killed within 5 days, whereas those exposed to an intermediate concentration of DOX (mid-DOX region) began to die on day 5 (Fig. 2e). On day 8, DOX-resistant (DOXR) cells appeared and proliferated in the mid-DOX region. On day 11, PACCs appeared in the mid-DOX region (Figure 2d, e), suggesting that they emerge from stressful but tolerable conditions on the chip in areas where an intermediate concentration of DOX is perfused.

Cells were collected from the chip on day 12 and incubated with medium containing DOX (0.05 μM) for 7 days in 24 wells to remove non-resistant cells that might have originated from the low-DOX region (Fig. 2a, b). Then, the DOXR cells were separated from the PACCs using FACS. The FACS cell cycle analysis showed that the proportions of polyploidy (cells greater than 4N+) in the WT cells, DOXR cells, and PACCs were 2, 15, and 40%, respectively (Fig. 2f–h). PACCs showed lower susceptibility to DOX than the WT and DOXR cells (Fig. 2i–k). Taken

together, these results suggest that the CDRA chip can rapidly induce the development of DOX-resistant PACCs.

PACCs accelerate cancerous growth and tumor progression in TNBC

To better define the oncogenic properties of PACCs, including chemoresistance in TNBC, we examined the effect of PACCs on cancer progression. Compared with WT cells, PACCs showed a higher rate of proliferation and a higher proportion of Ki67-positive cells (Fig. 3a, b). An *in vitro* wound-healing assay showed PACCs migrated faster than WT cells, suggesting that the development of PACCs could be a determinant of the migration capacity of TNBC (Fig. 3c).

To ascertain whether the PACCs augmented tumorigenicity and conferred DOX-resistance *in vivo*, we generated an animal model of TNBC by subcutaneously injecting mice with either WT cells or PACCs and treating the tumor-bearing mice with either vehicle or DOX (Fig 3d). Irrespective of DOX treatment, the mice injected with PACCs showed much larger tumors compared to the mice injected with WT cells (Fig. 3e). The tumor volume of PACCs treated with DOX and vehicle did not differ significantly ($p > 0.05$), but the tumor volume of WT cells treated with DOX was significantly smaller than that of WT cells treated with vehicle ($p < 0.001$) (Fig. 3f). This finding is supported by both hematoxylin and eosin (H&E) staining (Fig. 3g, top) and immunohistochemical staining for proliferating cell nuclear antigen (PCNA) (Fig. 3g, bottom) in the tumor tissues, which show that the cell density and proliferation of the PACCs were not reduced by DOX treatment, unlike those of WT cells. Therefore, the PACCs in TNBC developed in the CDRA chip significantly enhanced carcinogenesis, and tumors containing the PACCs were no longer sensitive to DOX.

Because the clinical implications of PACCs are still being evaluated, we analyzed the occurrence of PACCs in human TNBC patients. A tissue microarray (TMA) (n=130) found PACCs only in TNBC patient tissues but not in normal breast tissue (Fig. 3h and Supplementary Fig. 1a). In addition, the number of PACCs in each tissue correlated with tumor grade (Fig. 3i). Therefore, TNBC contains PACCs in proportion to tumor grade, and the formation of PACCs in TNBC contributes to tumor progression and malignancy.

NUPR1 is a key mediator of chemoresistance in PACCs

To elucidate the mechanism underlying the chemoresistance and oncogenic capacity of PACCs, we performed an RNA sequencing (RNA-seq)-based transcriptome analysis to identify genes differentially expressed between WT cells and PACCs. Among the genes whose expression was significantly altered (fold change cut-off = 2), 1,212 were upregulated and 1,602 were downregulated in PACCs (Fig. 4a). A DAVID gene ontology term analysis of genes upregulated

in PACCs (false discovery rate < 0.05) indicated that genes involved in cancer progression were most represented. An Ingenuity Pathway Analysis (IPA) revealed that Nupr1, whose upregulation is associated with malignancy of cancer and the chemoresistance network(*30*), was top-ranked, and antioxidant signaling was the most enriched pathway along with other cancer-promoting signaling such as tumor necrosis factor receptor 2, mitogen-activated protein kinase, and phospholipase signaling (Fig. 4b). Notably, the upstream regulator analysis in IPA revealed that Nupr1 is a high-rank regulator and is responsible for 4.4 % (53/1212) of the genes actively transcribed in PACCs (cut-off=1.5, $p < 0.05$) (Fig. 4c).

The clinical relevance of Nupr1 expression in TNBC was investigated using a cohort of patients treated with chemotherapy by performing a meta-analysis of all the datasets in Kaplan-Meier (KM) plotter (https://kmplot.com/analysis/index.php?p=service&cancer=breast) (*31*). The overall survival rate was significantly lower in patients with high Nupr1 mRNA expression than in patients whose Nupr1 mRNA expression was low (high, n=34; low, n=32; p =0.037) (Fig. 4d). Similarly, in other datasets (GSE12093 (*32*) and GSE16391 (*33*)), chemotherapy-treated breast cancer patients with significantly lower survival rates expressed higher level of Nupr1 (p =0.027 and 0.0003, respectively) (Fig. 4e and Supplementary Fig. 2a), suggesting that high Nupr1 expression is associated with poor clinical outcomes among TNBC patients.

Consistent with RNA-seq analysis of PACCs, increased expression of Nupr1 in both PACCs and PACCs-derived xenografts was observed in reverse transcriptase-quantitative polymerase chain reaction (RT-qPCR) (Fig. 4f). mRNA level of Nupr1 was barely detectable in the WT cells and WT cell-derived tumor tissues (Fig. 4f). Moreover, transactivation activity of the Nupr1 promoter was highly elevated in PACCs but not in WT cells (Fig 4g). These results indicate that Nupr1 expression is highly enhanced in PACCs. Silencing Nupr1 expression abolished the cell viability of DOX-treated PACCs, but it did not decrease the cell viability of vehicle-treated PACCs, suggesting that Nupr1 depletion could eliminate DOX resistance in PACCs (Fig. 4h and Supplementary Fig. 2b). Regardless of DOX-treatment, Nupr1 depletion did not affect the chemosensitivity of WT cells. These results suggest that Nupr1 upregulation may be a major driver of chemoresistance in PACCs.

To define the potential role of Nupr1 in mediating chemoresistance in TNBC, we treated WT cells and PACCs with ZZW-115, a Nupr1 inhibitor that alters its nuclear localization (*34*), in the absence or presence of DOX. ZZW-115 treatment led to re-sensitization of PACCs to DOX in a dose-dependent manner, whereas the WT cells merely responded to ZZW-115 (Fig. 4i). Delocalization of Nupr1 and increased cell death caused by ZZW-115 were confirmed by immunocytochemistry (Supplementary Fig. 2c) and active caspase-3 and poly (ADP-ribose)

polymerase (PARP) cleavage (Fig. 4j). To further verify whether Nupr1 inhibition could overcome DOX resistance and enhance drug response in PACCs, we treated xenograft model mice with DOX and two doses of ZZW-115 (Fig. 4k–o). The addition of ZZW-115 to DOX in the xenograft models reduced the tumor volume compared with the DOX-only-treated tumors (-469.5±25.20 mm^3 (2.5 mg/kg) and -627.2±15.36 (5.0 mg/kg)) (Fig. 4l–n) and elicited abundant cell death (Fig. 4o). Therefore, our data suggested that Nupr1 inhibition overcomes the chemoresistance of highly aggressive, chemoresistant PACCs in xenograft model mice.

HDAC11 suppression leads to Nupr1 upregulation in PACCs

To gain insights into the molecular mechanism underlying Nupr1 upregulation in PACCs, we aimed to identify a potent regulator of its gene expression. Because epigenetic alterations affect gene expression and are usually associated with cancer progression (*35*), we first examined the DNA methylation status of the Nupr1 promoter region. However, we did not find any remarkable changes in promoter methylation between WT cells and PACCs (Supplementary Fig. 3a). Intriguingly, chromatin immunoprecipitation (ChIP)-qPCR using the histone H3 at lysine 27 (H3K27)-acetylation antibody revealed H3K27 acetylation in PACCs, specifically in promoter region 3 (Fig. 5a). Spurred by our finding of enriched acetylation in PACCs, we attempted to identify a putative epigenetic regulator, such as a histone acetyltransferase (HAT) or HDAC that could be involved in the increased acetylation of Nupr1. An RNA-seq analysis of HATs and HDACs in WT cells and PACCs showed almost no detectable mRNA expression of Hdac11 in PACCs (Fig. 5b and Supplementary Fig. 3b), which we confirmed by RT-qPCR (Fig. 5c). Hdac11 expression was also dramatically reduced in tumors from PACCs-derived xenografts compared with tumors derived from WT cells (Fig. 5d). In addition, the protein expression of NUPR1 and HDAC11 was inversely correlated in PACCs and WT cells (Supplementary Fig. 3c, d), suggesting that low levels of HDAC11 in PACCs might contribute to the upregulation of Nupr1 through enriched acetylation in its promoter region. Indeed, forced expression of HDAC11 elicited a dramatic reduction in H3K27 acetylation in the PACCs promoter region (Fig. 5f), which reduced the mRNA expression of Nupr1 in a dose-dependent manner not seen in the parental WT cells (Fig. 5e) and also greatly impaired the promoter activity in the PACCs (Fig. 5g). These data clearly demonstrate that HDAC11 mediates Nupr1 promoter deacetylation, underscoring that the suppressed expression of HDAC11 in PACCs allows Nupr1 to escape deacetylation and thereby causes its aberrant high expression.

In a TMA of TNBC patient tissues (n=130), we verified that, as tumor grade increased, NUPR1 expression increased and HDAC11 expression decreased (Fig. 5h). In addition, a Kaplan Meier plot analysis of breast cancer patients (n=500, HER negative) from GSE25066 (*36*) showed

that patients with low Hdac11 expression had significantly shorter survival times than patients with high Hdac11 expression after chemotherapy (Supplementary Fig. 3e). Thus, these data emphasize that Nupr1 is inversely correlated with Hdac11 level in TNBC patients, and that the epigenetic dysregulation of Nupr1 caused by low HDAC11 level causes the chemoresistance that dictates the development of PACCs in TNBC.

Discussion

TNBC is the most aggressive subtype of breast cancer, and chemotherapy is a mainstay of treatment. However, chemoresistance is common and contributes to the long-term survival of TNBC patients (*37*). Therefore, novel strategies are urgently needed to enhance the clinical benefit of chemotherapy. In this work, we provide compelling evidence that cells in the PACC state obtained from a CDRA chip acquired drug resistance as compared to WT cells. We also identified a mechanism for that drug resistance through epigenetic control of the NUPR1/HDAC11 axis in TNBC. PACCs and PACCs-derived tumor tissues demonstrated dramatic, high-level expression of Nupr1, which was consistent with the poor clinical outcomes, including low overall survival (OS) and disease-free survival (DFS), found in chemotherapy-treated TNBC patients with high Nupr1. We also demonstrated that high Nupr1 expression in PACCs is induced by acetylation of the Nupr1 promoter through the aberrantly restricted expression of HDAC11. The identification of Nupr1 as a novel epigenetic target of HDAC11 in PACCs helps to explain how PACCs acquire chemoresistance. HDAC11 is the most recently discovered HDAC, and its pathophysiological role is poorly understood. For example, HDAC11 has a positive correlation with tumor growth, but its incongruously high expression also conferred longer DFS and OS in pancreatic tumor patients (*38*). HDAC11 is overexpressed in certain cancer cell lines, including prostatic (PC-3) (*39*), ovarian (SK-OV-3) (*19*), and breast cancer (MCF-7) cells (*40*), and HDAC11 inhibition has shown beneficial effects in neuroblastoma cells (*41*) and Hodgkin lymphoma (*42*). However, HDAC11 expression is inversely correlated with high-risk uveal melanomas and gliomas (*23*), and HDAC11 knockout mice have increased lymphoma tumor growth (*24*). HDAC11 inhibition promotes breast cancer cell metastasis (*43*). In basal-like breast cancer cells with decreased HDAC11 expression, overexpression of HDAC11 did not inhibit tumor growth but did inhibit invasion and metastasis (*44*). In addition, the Cancer Genome Atlas shows that Hdac11 promoter methylation is associated with a poor prognosis of ovarian cancer patients (*45*), suggesting the need for in-depth studies of the specific mechanisms of HDAC11 in specific tumors. In this study, we observed extremely low HDAC11 expression in PACCs compared with WT cells, and we confirmed that its expression is much lower in patients with high-grade TNBC tumors than in those with low-grade tumors. We also found a positive

correlation between its expression and disease-free survival (Supplementary Fig. 3e). Because we identified that NUPR1 as a novel target of HDAC11, and drastically decreasing the expression of HDAC11 causes aberrantly high expression of NUPR1 in PACCs and TNBC patients (Fig. 5h), it is plausible that limited expression of HDAC11 leads to a high NUPR1 level to acquire chemoresistance. It is also possible that HDAC11 expression may be suppressed in chemoresistant TNBC cells by a specific regulator that requires further elucidation.

In breast cancer, aberrations in histone modification such as acetylation have been shown to be important for tumor progression and have been proposed as a promising therapeutic target (*46*). HDACs have been an attractive therapeutic strategy for restoring both acetylation and gene expression, with the potential benefit of being better tolerated than cytotoxic chemotherapy. Epigenetic modulation has also been hypothesized as a mechanism of chemoresistance. In this study, we showed that NUPR1 overexpression upon acquisition of DOX resistance leads to upregulation of cancer-promoting signaling. Moreover, we demonstrated that NUPR1 inhibition with ZZW-115 reconstitutes the drug sensitivity of PACCs and HDAC11 overexpression inhibited Nupr1 expression by eliciting deacetylation of the Nupr1 promoter region in PACCs. Thus, despite the promising anti-tumor effects of HDAC inhibitors (HDACi) in preclinical models, our results suggest the importance of evaluating HDACi as therapeutic candidates in the context of drug-resistance, as well as cells in the PACC state in TNBC.

Our results demonstrate that clinically meaningful PACCs can be obtained within a few weeks using the CDRA chip to mimic the spatiotemporally heterogeneous ecosystem of cancer cells in the tumor tissues of patients receiving chemotherapy. Although PACCs are often found in cancer patient tissues, their isolation is technically difficult, which is an obstacle to studying how they contribute to chemoresistance in cancer patients. Therefore, our methodology, examining the expression of genes involved in the chemoresistance of chip-derived PACCs and comparing those results with gene expression data from patient tissues in which PACCs are found, opens a new avenue for understanding the mechanism of chemoresistance caused by PACCs. Because the chip requires approximately 15,000 cells each, it can be also used to predict PACC formation in patients prior to chemotherapy (*47*).

Materials and Methods

Fabrication of the CDRA chip

The CDRA chip was fabricated using soft lithography, as previously described[11,43]. The chip contained a patterned array of 444 hexagonal microchambers, each with a diameter of 200 μm. In

the outermost chambers, 5-μm-wide channels allowed medium with and without DOX to perfuse into the interior microchambers. Each interior microchamber had three gates through which the cells could move into the connected chambers.

Cell culture

The MDA-MB-231 TNBC cell line was purchased from ATCC (Manassas, VA, USA) and cultured in RPMI-1640 medium (HyClone, Logan, UT, USA) supplemented with 10% fetal bovine serum (HyClone), 100 units per mL of penicillin (Life Technologies, Carlsbad, CA, USA), and 100 μg/mL of streptomycin (Life Technologies) and maintained at 37□ with 5% CO_2.

Operation of the CDRA chip

The chip was prepared before cell seeding as described before[11]. A total of 1×10^5 cells/10 μL was suspended in culture medium, and 1 μL of the solution was gently added to the chip using a pipette with a tip through the cell seeding hole. The hole was plugged with a sterilized stainless pin, and the chip was incubated at 37□ with 5% CO_2 overnight. The next day, 250 μL of culture medium and culture medium containing 1.5 μM DOX were added to two of the diagonal reservoirs, and 50 μL of culture medium was added to the rest of the diagonal reservoirs. The fresh culture medium and drug were replaced every day. After 11 days, trypsin (Gibco) was added to the chip, which was incubated at 37□ for 5 min. The detached cells were flushed out of the chip and collected from the reservoirs by injecting 1 mL of culture medium through the seeding hole with a needle-free syringe. To remove non-resistant cells, the collected cells were grown in medium containing 0.05 μM DOX for one week (Fig. 2a).

PACCs separation using FACS

DOXR cells were seeded in a 10-mm cell culture dish for 1 day and then stained with 5 μg/mL of Hoechst-33342 at 37□ for 5 min and analyzed on a FACSAria™ Fusion (BD Biosciences, Franklin Lakes, NJ, USA).

Cell cycle analysis using FACS

WT, DOXR, and PACCs were collected in a 15 ml tube and fixed in pre-cooled 70% ethanol at 4□ for 1 h. The cells were permeabilized in 0.25% Triton X-100 with phosphate buffered saline (PBS, pH 7.4) at 4□ for 15 min and then stained with 20 μg/mL of propidium iodide (Sigma-Aldrich) containing 10 μg/mL of ribonuclease A at room temperature for 30 min. The stained cells were analyzed in the FACSAria™ Fusion.

DOX efflux

About 1 × 10^5 cells were incubated in a 6-well plate (Corning Inc.) containing RPMI-1640 medium with 5 μM (final concentration) DOX at 37□ for 3 h, and then the medium was replaced with fresh RPMI-1640 without DOX. After 24 h, fluorescent images were captured using a DeltaVision Elite microscope (GE Healthcare). Then, 10 cells were randomly chosen from the images, and their fluorescence intensity at 585 nm was analyzed using ImageJ (NIH, Bethesda, MD, USA).

Cell viability

To assess the cytotoxic effects of DOX on cells, approximately10^3 cells were incubated in a 96-well plate with DOX (0–1 μM) for 72 h at 37□. Their viability was measured using EZ-Cytox reagent (Daeillab Service, Seoul, Korea). The percentage of viable cells was calculated by dividing the number of viable cells at each DOX concentration by the number of cells cultured without DOX.

RNA sequencing

Total RNA from MDA-MB-231 cells and PACCs was extracted using a RNeasy Mini Kit (Qiagen, Germantown, MD, USA). RNA sequencing was performed on the NextSeq 500 sequencing platform (Illumina, San Diego, CA, USA). Biological functions were determined using IPA web-based bioinformatics software (Qiagen). A two-fold change in PACC gene expression was used as the cut-off value indicating a significant change in expression compared with that in MDA-MB-231 cells.

Antibodies and Chemicals

Anti-PCNA (ab29), Ki67 (ab15580), NUPR1 (ab234696), and active-Caspase 3 (ab2302) antibodies were acquired from Abcam (Cambridge, UK). Anti-HDAC11 (H4539) and HDAC11 (WH0079885M1) antibodies were acquired from Sigma-Aldrich. Anti-PARP (9542S) antibody was obtained from Cell Signaling Technology (Danvers, MA, USA). Anti-ACTIN (sc-47778) antibody was obtained from Santa Cruz Biotechnology (Dallas, TX, USA). Dimethyl sulfoxide (D2447), ZZW-115 (HY-111838A), and doxorubicin (D1515) were acquired from Sigma-Aldrich.

Tissue Microarray and Immunohistochemistry

Slides of TNBC and normal tissues were obtained from US Biomax (BR1301) (Derwood, MD, USA). For staining, each slide was deparaffinized and permeabilized using 0.25% Triton X-100

in PBS for 2 h. The slides were immunostained using primary antibodies and incubated overnight at 4°C and then incubated for 1 h at room temperature with secondary antibodies (Alexa Fluor-488 or -546). Nuclei were counterstained with 4′,6-diamidino-2-phenylindole. Z-stacked images of the stained tissues were acquired using a ZEISS LSM 710 confocal microscope (Oberkochen, Germany).

Western blot

Transfected cells were washed with PBS and treated with ice-cold lysis buffer (50 mM Tris-Cl, pH7.4; 150 mM NaCl; 1 mM EDTA; 0.5% Triton X-100; 1.5 mM Na_3VO_4; 50 mM sodium fluoride; 10 mM sodium pyrophosphate; 10 mM glycerophosphate; 1 mM phenylmethylsulfonyl fluoride, and protease cocktail (Calbiochem, San Diego, CA, USA)). Equal amounts of proteins were denatured, resolved on SDS-PAGE, and transferred to nitrocellulose membranes (Pall Life Science, Port Washington, NY, USA) (*48*).

RT-qPCR

To compare the mRNA levels of WT cells and PACCs, RT-qPCR was performed. Total RNA was isolated from cells or tumors using a Mini BEST Universal RNA Extraction Kit (Takara, Shiga, Japan). cDNA was prepared from total RNA by reverse transcription using oligo-dT primers (Takara). RT-qPCR was conducted using SoFast EvaGreen Super Mix (Bio-Rad, Hercules, CA, USA) according to the manufacturer's instructions. glyceraldehyde 3-phosphate dehydrogenase (*Gapdh*) was used as an internal control for quantitation of target gene expression. A total reaction mixture with a volume of 20 µl was amplified in a 96-well PCR plate (Bio-Rad). The primer sets used are listed in Supplementary Table 1.

Luciferase assay

MDA-MB-231 cells and PACCs were plated in culture plates and transfected with 100 ng of *Nupr1*-promoter-luciferase reporter and 30 ng of *Renilla* reporter vector in 6-well plates and then incubated for 24 h (*49*). The cells were lysed, and luciferase assays were performed using a dual luciferase assay kit (Promega, Madison, WI, USA) according to the manufacturer's instructions. The transfection efficiency was normalized against *Renilla* luciferase activity, and the transfection of genes was confirmed using immunoblotting. All assays were performed at least in triplicate.

ChIP assay

ChIP assays were performed using a ChIP Assay Kit (cat. 17-259; Millipore, Temecula, CA, USA) according to the manufacturer's instructions. Primers from multiple sites relative to the

transcription start site were designed and pretested in both the input and ChIP samples. Purified DNA was subjected to qPCR with primers against the *Nupr1* promoter region. The primer sets used are listed in Supplementary Table 1.

Survival analysis

The KM plots were taken from https://kmplot.com/analysis/index.php?p=service&cancer=breast (*33*). We chose TNBC patients as follows: ER status IHC: ER-negative; ER status array: ER-negative; PR status IHC: PR negative; and HER2 status array: HER2 negative for meta-analysis and retrieved from the NCBI GEO database (GSE12093 (*32*), GSE16391 (*33*), and GSE25066 (*36*)).

Animal

All animal experiments were reviewed and approved by the Institutional Animal Care and Use Committee (IACUC) of Sungkyunkwan University School of Medicine (SUSM, SKKUIACUC2021-03-47-1). All experimental procedures were performed according to the regulations of the IACUC guidelines of Sungkyunkwan University.

Xenograft

Procedures for the animal studies were described previously (*50*). Briefly, 6- to 8-week-old female Balb/c nude mice (Orientbio Inc., Seongnam, Korea) were housed in laminar-flow cabinets under specific pathogen-free conditions. Approximately 1×10^7 cells of WT cells or PACCs were resuspended in 100 μl of a 1:1 ratio of PBS and Matrigel (Corning Inc., Corning, NY, USA, #354234) and subcutaneously injected into each mouse. The tumor size was monitored every three days using calipers, and the tumor volume (V) was calculated using the formula $V = (L \times W^2)/2$, where L was the length and W was the width of the tumor. When the tumor volume reached 150 mm^3, the tail veins of the mice were injected with 2 mg/kg of DOX for Fig. 3d–g or 2.5 mg/kg or 5.0 mg/kg of ZZW-115 (daily) with and without 2 mg/kg of DOX for Fig. 4k–o.

Statistical analysis

All statistical analyses were performed using Prism 8 (GraphPad Software, San Diego, CA, USA). In general, statistical analyses were performed using ANOVA and Student's *t*-test. Two-tailed and unpaired *t*-tests were used to compare two conditions. Two-way ANOVA with Tukey's post hoc test was used to analyze multiple groups. One-way ANOVA with Bonferroni's post hoc test was used for comparisons of ages and genotypes. Data are represented as mean ± standard

error of the mean (SEM) unless otherwise noted, with asterisks indicating *$p < 0.05$, **$p < 0.01$, and ***$p < 0.001$.

References

1. A. A. Jazaeri, C. S. Awtrey, G. V. Chandramouli, Y. E. Chuang, J. Khan, C. Sotiriou, O. Aprelikova, C. J. Yee, K. K. Zorn, M. J. Birrer, J. C. Barrett, J. Boyd, Gene expression profiles associated with response to chemotherapy in epithelial ovarian cancers. *Clin. Cancer Res.* **11**, 6300-6310 (2005).
2. G. H. Heppner, B. E. Miller, Tumor heterogeneity: biological implications and therapeutic consequences. *Cancer Metastasis Rev.* **2**, 5-23 (1983).
3. J. Chen, N. Niu, J. Zhang, L. Qi, W. Shen, K. V. Donkena, Z. Feng, J. Liu, Polyploid Giant Cancer Cells (PGCCs): The Evil Roots of Cancer. *Curr. Cancer Drug Targets* **19**, 360-367 (2019).
4. S. Zhang, I. Mercado-Uribe, Z. Xing, B. Sun, J. Kuang, J. Liu, Generation of cancer stem-like cells through the formation of polyploid giant cancer cells. *Oncogene* **33**, 116-128 (2014).
5. S. Zhang, I. Mercado-Uribe, J. Liu, Tumor stroma and differentiated cancer cells can be originated directly from polyploid giant cancer cells induced by paclitaxel. *Int. J. Cancer* **134**, 508-518 (2014).
6. L. Jia, S. Zhang, Y. Ye, X. Li, I. Mercado-Uribe, R. C. Bast, Jr., J. Liu, Paclitaxel inhibits ovarian tumor growth by inducing epithelial cancer cells to benign fibroblast-like cells. *Cancer Lett.* **326**, 176-182 (2012).
7. S. Islam, A. L. Paek, M. Hammer, S. Rangarajan, R. Ruijtenbeek, L. Cooke, E. Weterings, D. Mahadevan, Drug-induced aneuploidy and polyploidy is a mechanism of disease relapse in MYC/BCL2-addicted diffuse large B-cell lymphoma. *Oncotarget* **9**, 35875-35890 (2018).
8. Z. Zhang, X. Feng, Z. Deng, J. Cheng, Y. Wang, M. Zhao, Y. Zhao, S. He, Q. Huang, Irradiation-induced polyploid giant cancer cells are involved in tumor cell repopulation via neosis. *Mol. Oncol.* **15**, 2219-2234 (2021).

9. H. J. Ahn, Y. S. Kim, J. U. Kim, S. M. Han, J. W. Shin, H. O. Yang, Mechanism of taxol-induced apoptosis in human SKOV3 ovarian carcinoma cells. *J. Cell. Biochem.* **91**, 1043-1052 (2004).

10. N. Niu, J. Zhang, N. Zhang, I. Mercado-Uribe, F. Tao, Z. Han, S. Pathak, A. Multani, J. Kuang, J. Yao, Linking genomic reorganization to tumor initiation via the giant cell cycle. *Oncogenesis* **5**, e281-e281 (2016).

11. T. A. Martin, A. X. Li, A. J. Sanders, L. Ye, K. Frewer, R. Hargest, W. G. Jiang, NUPR1 and its potential role in cancer and pathological conditions (Review). *Int. J. Oncol.* **58**, (2021).

12. T. Hamidi, C. E. Cano, D. Grasso, M. N. Garcia, M. J. Sandi, E. L. Calvo, J. C. Dagorn, G. Lomberk, R. Urrutia, S. Goruppi, A. Carracedo, G. Velasco, J. L. Iovanna, Nupr1-aurora kinase A pathway provides protection against metabolic stress-mediated autophagic-associated cell death. *Clin. Cancer Res.* **18**, 5234-5246 (2012).

13. L. Brannon-Peppas, B. Ghosn, K. Roy, K. Cornetta, Encapsulation of nucleic acids and opportunities for cancer treatment. *Pharm. Res.* **24**, 618-627 (2007).

14. D. W. Clark, A. Mitra, R. A. Fillmore, W. G. Jiang, R. S. Samant, O. Fodstad, L. A. Shevde, NUPR1 interacts with p53, transcriptionally regulates p21 and rescues breast epithelial cells from doxorubicin-induced genotoxic stress. *Curr. Cancer Drug Targets* **8**, 421-430 (2008).

15. A. J. Vincent, S. Ren, L. G. Harris, D. J. Devine, R. S. Samant, O. Fodstad, L. A. Shevde, Cytoplasmic translocation of p21 mediates NUPR1-induced chemoresistance: NUPR1 and p21 in chemoresistance. *FEBS Let.t* **586**, 3429-3434 (2012).

16. S.-H. Jung, A. Lee, S.-H. Yim, H.-J. Hu, C. Choe, Y.-J. Chung, Simultaneous copy number gains of NUPR1 and ERBB2 predicting poor prognosis in early-stage breast cancer. *BMC Cancer* **12**, 382 (2012).

17. Y. Mu, X. Yan, D. Li, D. Zhao, L. Wang, X. Wang, D. Gao, J. Yang, H. Zhang, Y. Li, Y. Sun, Y. Wei, Z. Zhang, X. Chang, Z. Yao, S. Tian, K. Zhang, L. S. Terada, Z. Ma, Z. Liu, NUPR1 maintains autolysosomal efflux by activating SNAP25 transcription in cancer cells. *Autophagy* **14**, 654-670 (2018).

18. D. Gong, Z. Zeng, F. Yi, J. Wu, Inhibition of histone deacetylase 11 promotes human liver cancer cell apoptosis. *Am. J. Transl. Res.* **11**, 983-990 (2019).

19. L. Zhou, X. Xu, H. Liu, X. Hu, W. Zhang, M. Ye, X. Zhu, Prognosis Analysis of Histone Deacetylases mRNA Expression in Ovarian Cancer Patients. *J. Cancer* **9**, 4547-4555 (2018).

20. L. Yue, V. Sharma, N. P. Horvat, A. A. Akuffo, M. S. Beatty, C. Murdun, C. Colin, J. M. R. Billington, W. E. Goodheart, E. Sahakian, L. Zhang, J. J. Powers, N. E. Amin, Q. T. Lambert-Showers, L. N. Darville, J. Pinilla-Ibarz, G. W. Reuther, K. L. Wright, C. Conti, J. Y. Lee, X. Zheng, P. Y. Ng, M. W. Martin, C. G. Marshall, J. M. Koomen, R. L. Levine, A. Verma, H. L. Grimes, E. M. Sotomayor, Z. Shao, P. K. Epling-Burnette, HDAC11 deficiency disrupts oncogene-induced hematopoiesis in myeloproliferative neoplasms. *Blood* **135**, 191-207 (2020).

21. Z. Huang, W. Zhou, Y. Li, M. Cao, T. Wang, Y. Ma, Q. Guo, X. Wang, C. Zhang, C. Zhang, W. Shen, Y. Liu, Y. Chen, J. Zheng, S. Yang, Y. Fan, R. Xiang, Novel hybrid molecule overcomes the limited response of solid tumours to HDAC inhibitors via suppressing JAK1-STAT3-BCL2 signalling. *Theranostics* **8**, 4995-5011 (2018).

22. K. Liu, R. Zou, W. Cui, M. Li, X. Wang, J. Dong, H. Li, H. Li, P. Wang, X. Shao, W. Su, H. C. S. Chan, H. Li, S. Yuan, Clinical HDAC Inhibitors Are Effective Drugs to Prevent the Entry of SARS-CoV2. *ACS Pharmacol. Transl. Sci.* **3**, 1361-1370 (2020).

23. N. Dali-Youcef, S. Froelich, F. M. Moussallieh, S. Chibbaro, G. Noël, I. J. Namer, S. Heikkinen, J. Auwerx, Gene expression mapping of histone deacetylases and co-factors, and correlation with survival time and 1H-HRMAS metabolomic profile in human gliomas. *Sci. Rep.* **5**, 9087 (2015).

24. E. Sahakian, J. J. Powers, J. Chen, S. L. Deng, F. Cheng, A. Distler, D. M. Woods, J. Rock-Klotz, A. L. Sodre, J. I. Youn, K. V. Woan, A. Villagra, D. Gabrilovich, E. M. Sotomayor, J. Pinilla-Ibarz, Histone deacetylase 11: A novel epigenetic regulator of myeloid derived suppressor cell expansion and function. *Mol. Immunol.* **63**, 579-585 (2015).

25. L. Y. Yeo, H.-C. Chang, P. P. Y. Chan, J. R. Friend, Microfluidic Devices for Bioapplications. *Small* **7**, 12-48 (2011).

26. A. Wu, K. Loutherback, G. Lambert, L. Estévez-Salmerón, T. D. Tlsty, R. H. Austin, J. C. Sturm, Cell motility and drug gradients in the emergence of resistance to chemotherapy. *Proc. Nat.l Acad. Sci. U. S. A.* **110**, 16103-16108 (2013).

27. J. Han, W. Lim, D. You, Y. Jeong, S. Kim, J. E. Lee, T. H. Shin, G. Lee, S. Park, Chemoresistance in the Human Triple-Negative Breast Cancer Cell Line MDA-MB-231 Induced by Doxorubicin Gradient Is Associated with Epigenetic Alterations in Histone Deacetylase. *J. Oncol.* **2019**, 1345026 (2019).

28. J. Han, Y. Jun, S. H. Kim, H.-H. Hoang, Y. Jung, S. Kim, J. Kim, R. H. Austin, S. Lee, S. Park, Rapid emergence and mechanisms of resistance by U87 glioblastoma cells to

doxorubicin in an in vitro tumor microfluidic ecology. *Proc. Nat.l Acad. Sci. U. S. A.* **113**, 14283-14288 (2016).

29. K.-C. Lin, Y. Sun, G. Torga, P. Sherpa, Y. Zhao, J. Qu, S. R. Amend, K. J. Pienta, J. C. Sturm, R. H. Austin, An in vitro tumor swamp model of heterogeneous cellular and chemotherapeutic landscapes. *Lab Chip* **20**, 2453-2464 (2020).
30. L. Wang, J. Sun, Y. Yin, Y. Sun, J. Ma, R. Zhou, X. Chang, D. Li, Z. Yao, S. Tian, K. Zhang, Z. Liu, Z. Ma, Transcriptional coregualtor NUPR1 maintains tamoxifen resistance in breast cancer cells. *Cell Death Dis.* **12**, 149 (2021).
31. A. Lánczky, B. Győrffy, Web-Based Survival Analysis Tool Tailored for Medical Research (KMplot): Development and Implementation. *J. Med. Internet. Res.* **23**, e27633 (2021).
32. Y. Zhang, A. M. Sieuwerts, M. McGreevy, G. Casey, T. Cufer, A. Paradiso, N. Harbeck, P. N. Span, D. G. Hicks, J. Crowe, R. R. Tubbs, G. T. Budd, J. Lyons, F. C. Sweep, M. Schmitt, F. Schittulli, R. Golouh, D. Talantov, Y. Wang, J. A. Foekens, The 76-gene signature defines high-risk patients that benefit from adjuvant tamoxifen therapy. *Breast Cancer Res. Treat.* **116**, 303-309 (2009).
33. C. Desmedt, A. Giobbie-Hurder, P. Neven, R. Paridaens, M. R. Christiaens, A. Smeets, F. Lallemand, B. Haibe-Kains, G. Viale, R. D. Gelber, M. Piccart, C. Sotiriou, The Gene expression Grade Index: a potential predictor of relapse for endocrine-treated breast cancer patients in the BIG 1-98 trial. *BMC Med. Genomics* **2**, 40 (2009).
34. W. Lan, P. Santofimia-Castaño, M. Swayden, Y. Xia, Z. Zhou, S. Audebert, L. Camoin, C. Huang, L. Peng, A. Jiménez-Alesanco, A. Velázquez-Campoy, O. Abián, G. Lomberk, R. Urrutia, B. Rizzuti, V. Geli, P. Soubeyran, J. L. Neira, J. Iovanna, ZZW-115-dependent inhibition of NUPR1 nuclear translocation sensitizes cancer cells to genotoxic agents. *JCI Insight* **5**, e138117 (2020).
35. E. Baxter, K. Windloch, F. Gannon, J. S. Lee, Epigenetic regulation in cancer progression. *Cell & Bioscience* **4**, 45 (2014).
36. C. Hatzis, L. Pusztai, V. Valero, D. J. Booser, L. Esserman, A. Lluch, T. Vidaurre, F. Holmes, E. Souchon, H. Wang, M. Martin, J. Cotrina, H. Gomez, R. Hubbard, J. I. Chacón, J. Ferrer-Lozano, R. Dyer, M. Buxton, Y. Gong, Y. Wu, N. Ibrahim, E. Andreopoulou, N. T. Ueno, K. Hunt, W. Yang, A. Nazario, A. DeMichele, J. O'Shaughnessy, G. N. Hortobagyi, W. F. Symmans, A genomic predictor of response and survival following taxane-anthracycline chemotherapy for invasive breast cancer. *JAMA* **305**, 1873-1881 (2011).

37. C. Liedtke, C. Mazouni, K. R. Hess, F. Andre, A. Tordai, J. A. Mejia, W. F. Symmans, A. M. Gonzalez-Angulo, B. Hennessy, M. Green, M. Cristofanilli, G. N. Hortobagyi, L. Pusztai, Response to neoadjuvant therapy and long-term survival in patients with triple-negative breast cancer. *J. Clin. Oncol.* **26**, 1275-1281 (2008).

38. E. Klieser, R. Urbas, S. Stattner, F. Primavesi, T. Jager, A. Dinnewitzer, C. Mayr, T. Kiesslich, K. Holzmann, P. Di Fazio, D. Neureiter, S. Swierczynski, Comprehensive immunohistochemical analysis of histone deacetylases in pancreatic neuroendocrine tumors: HDAC5 as a predictor of poor clinical outcome. *Hum. Pathol.* **65**, 41-52 (2017).

39. W. Huo, F. Qi, K. Wang, Long noncoding RNA BCYRN1 promotes prostate cancer progression via elevation of HDAC11. *Oncol. Rep.* **44**, 1233-1245 (2020).

40. L. Gao, M. A. Cueto, F. Asselbergs, P. Atadja, Cloning and Functional Characterization of HDAC11, a Novel Member of the Human Histone Deacetylase Family. *J. Biol. Chem.* **277**, 25748-25755 (2002).

41. T. M. Thole, M. Lodrini, J. Fabian, J. Wuenschel, S. Pfeil, T. Hielscher, A. Kopp-Schneider, U. Heinicke, S. Fulda, O. Witt, A. Eggert, M. Fischer, H. E. Deubzer, Neuroblastoma cells depend on HDAC11 for mitotic cell cycle progression and survival. *Cell Death Dis.* **8**, e2635 (2017).

42. D. Buglio, N. M. Khaskhely, K. S. Voo, H. Martinez-Valdez, Y.-J. Liu, A. Younes, HDAC11 plays an essential role in regulating OX40 ligand expression in Hodgkin lymphoma. *Blood* **117**, 2910-2917 (2011).

43. P. L. Leslie, Y. L. Chao, Y. H. Tsai, S. K. Ghosh, A. Porrello, A. E. D. Van Swearingen, E. B. Harrison, B. C. Cooley, J. S. Parker, L. A. Carey, C. V. Pecot, Histone deacetylase 11 inhibition promotes breast cancer metastasis from lymph nodes. *Nat. Commun.* **10**, 4192 (2019).

44. C. Denkert, C. Liedtke, A. Tutt, G. von Minckwitz, Molecular alterations in triple-negative breast cancer-the road to new treatment strategies. *Lancet* **389**, 2430-2442 (2017).

45. Y. Dai, S. Chen, M. Kmieciak, L. Zhou, H. Lin, X. Y. Pei, S. Grant, The novel Chk1 inhibitor MK-8776 sensitizes human leukemia cells to HDAC inhibitors by targeting the intra-S checkpoint and DNA replication and repair. *Mol. Cancer Ther.* **12**, 878-889 (2013).

46. Y. Cheng, C. He, M. Wang, X. Ma, F. Mo, S. Yang, J. Han, X. Wei, Targeting epigenetic regulators for cancer therapy: mechanisms and advances in clinical trials. *Signal Transduct. Target. Ther.* **4**, 62 (2019).

47. L. A. Garraway, P. A. Jänne, Circumventing cancer drug resistance in the era of personalized medicine. *Cancer Discov.* **2**, 214-226 (2012).
48. S. H. Woo, B. Kim, S. H. Kim, B. C. Jung, Y. Lee, Y. S. Kim, Pulsed electromagnetic field potentiates etoposide-induced MCF-7 cell death. *BMB Rep.* **55**, 148-153 (2022).
49. S. H. Yu, S. Kim, Y. Kim, S. E. Lee, J. H. Park, G. Cho, J. C. Ha, H. Jung, S. M. Lim, K. Han, H. K. Lee, Y. C. Kang, C. H. Kim, Human umbilical cord mesenchymal stem cell-derived mitochondria (PN-101) attenuate LPS-induced inflammatory responses by inhibiting NFκB signaling pathway. *BMB Rep.* **55**, 136-141 (2022).
50. I. Hwang, C. K. Kim, H. R. Ko, K. W. Park, S. W. Cho, J. Y. Ahn, C-terminal domain of p42 Ebp1 is essential for down regulation of p85 subunit of PI3K, inhibiting tumor growth. *Sci. Rep.* **6**, 30626 (2016).

Acknowledgments

Funding: This work was equally supported by a National Research Foundation of Korea (NRF) grant (2016R1A5A2945889 to I.H. and J.I.A.) funded by the Ministry of Science, Information and Communication Technology, Future Planning (MSIP) of Korea and the Technology Innovation Program (20008413 to J.Z., Z.C., J.H., and S.P.) funded by the Ministry of Trade, Industry, & Energy (MOTIE) of Korea, and the Fostering Global Talents for Innovative Growth Program (P0008746 to W.L.) supervised by the Korea Institute for Advancement of Technology (KIAT).

Author contributions: S.P., R.H.A., and J.Y.A. conceived this study. W.L., I.H., J.Z., and Z.C. performed Experiments. W.L., I.H., J.Z., Z.C., S.K., J.H., and J.Y.A. analyzed results. W.L., I.H., S.P., J.Y.A. wrote the manuscript. B.K.K., J.E.L., S.L., K.J.P., S.R.A., R.H.A. revised and edited the manuscript.

Competing interests: The authors declare that they have no competing interests.

Data and materials availability: All data needed to evaluate the conclusions in the paper are present in the paper and/or the Supplementary Materials.

FIGURES

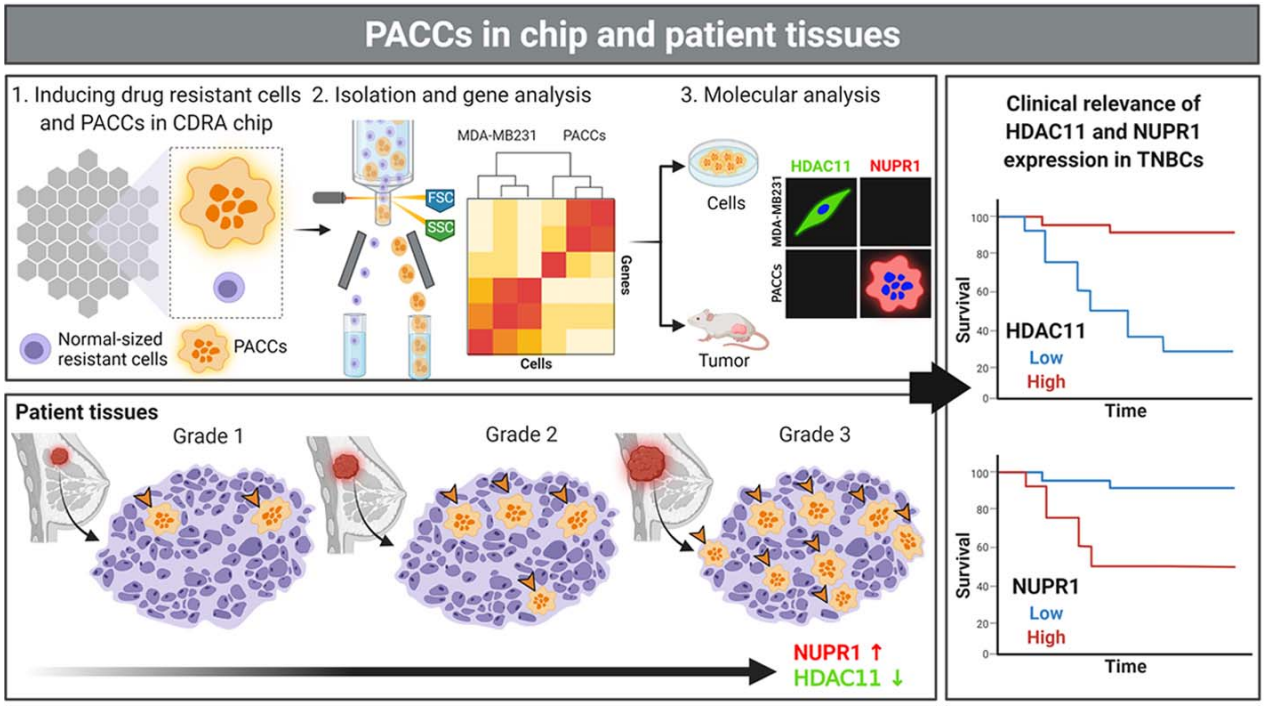

Fig. 1. Overall schematic of the experiment. Doxorubicin (DOX)-resistant triple negative breast cancer (TNBC) cells were induced from wild type (WT) TNBC cells by generating doxorubicin (DOX) and nutrient gradients in a Cancer Drug Resistance Accelerator (CDRA) chip[28]. Polyaneuploid cancer cells (PACCs) were isolated from the DOX-resistant TNBC cells using fluorescence-activated cell sorting (FACS), and their transcriptome was analyzed using RNA sequencing (RNA-seq). To better define the oncogenic properties of the PACCs, we examined their effect on cancer progression *in vivo* and *in vitro*. Also, we found that the rate of PACCs in TNBC patient tissues was positively associated with tumor grade. The roles of histone deacetylase 11 (HDAC11) and nuclear protein-1 (NUPR1) in DOX-resistance in PACCs were investigated using molecular analysis and the survival of patients with high/low NUPR1 expression.

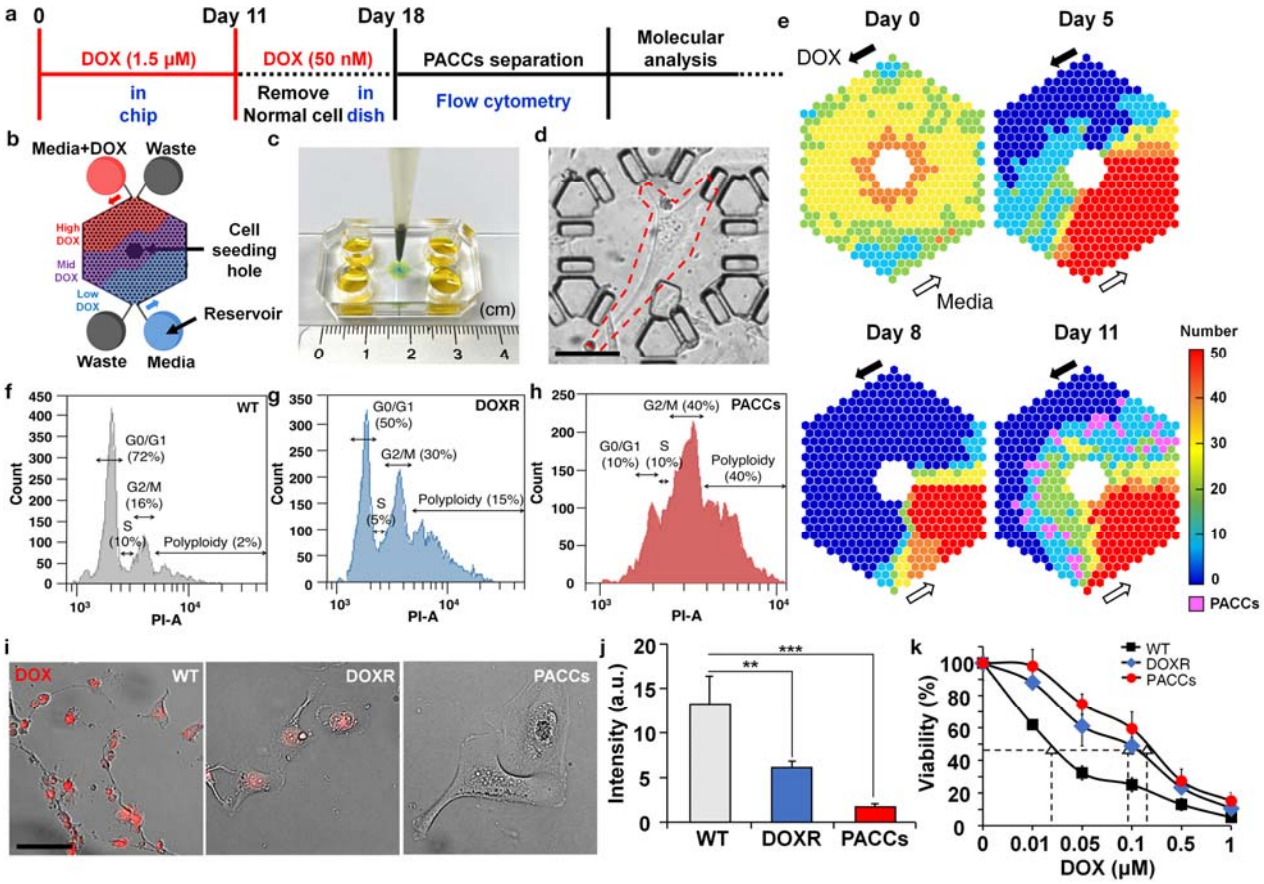

Fig. 2. Tracking PACCs induced by a DOX concentration-gradient in the CDRA chip and their cell cycle and drug resistance. (**a**) Experimental design. (**b**) Dimension of the chip. (**c**) Image of the CDRA chip. (**d**) PACCs (red dotted line) induced in the CDRA chip. (**e**) Tracking the number of live cells in each chamber of the chip for 11 days. PACCs are visible in some of the pink chambers on day 11. FACS analysis for the cell cycle of (**f**) WT cells, (**g**) DOXR cells, and (**h**) PACCs. (**i**) Red fluorescent intensity of WT cells, DOXR cells, and PACCs. Scale bars = 100 μm. (**j**) DOX efflux ability of WT cells, DOXR cells, and PACCs. $**p < 0.01$, $***p < 0.001$, two-tailed Student's *t*-test. (k) DOX sensitivity of WT cells (The half-maximal inhibitory concentration (IC_{50}) = 25 nM), DOXR cells (IC_{50} = 100 nM), and PACCs (IC_{50} = 200 nM).

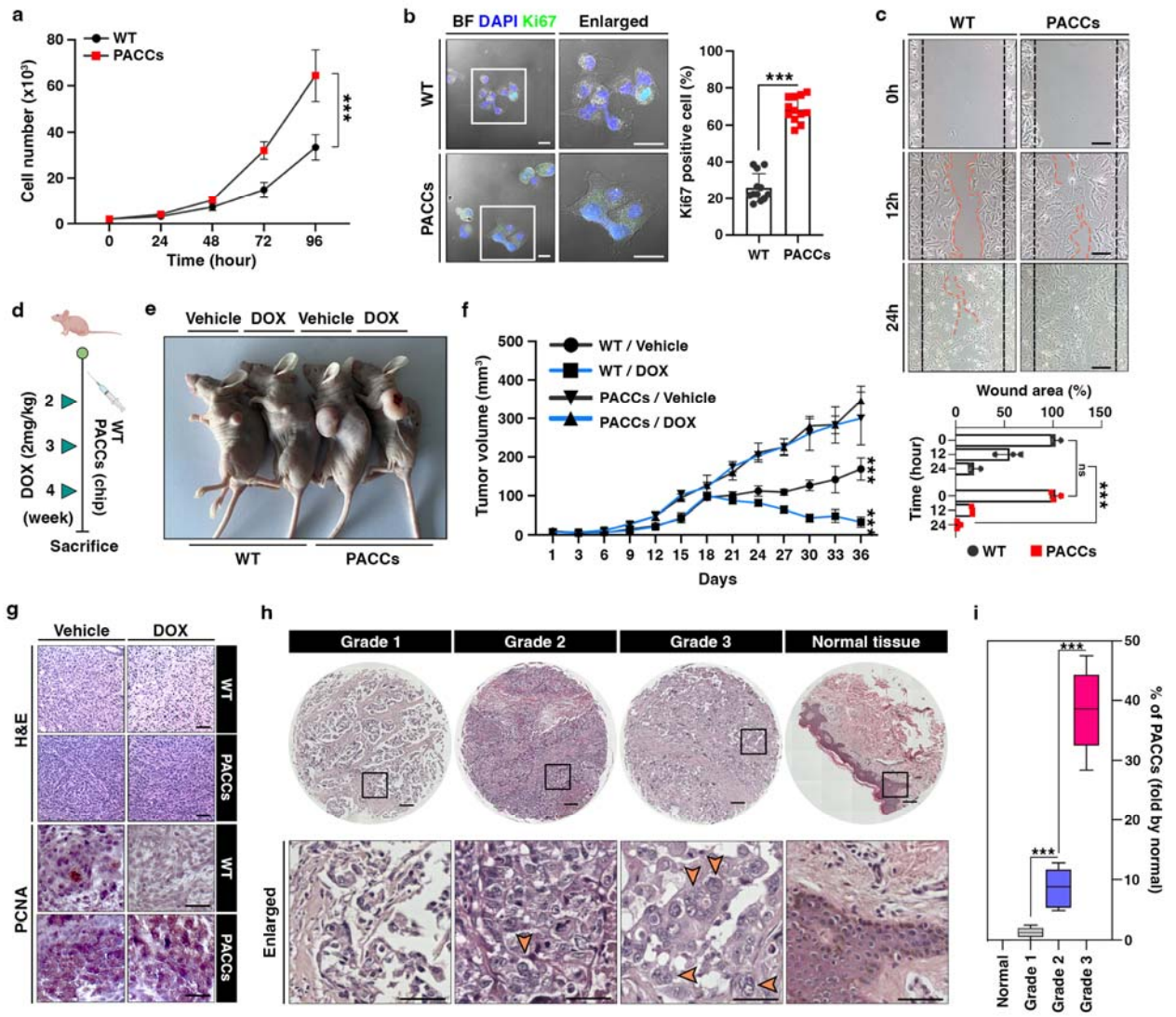

Fig. 3. PACCs accelerate cancerous growth and tumor progression in TNBC. (**a**) A proliferative assay was performed to examine the effect of PACCs on cell proliferation by cell counting. (**b**) Cells were stained with anti-Ki67 antibody (green) to measure their proliferative ability (left). The intensity of Ki67 was measured in eight randomly selected fields. Scale bar: 20 μm. (**c**) Representative images from wound healing assays from 0 h to 24 h. The black lines display the scratched outlines. The gap (orange) between cells was determined and shown as a bar graph (bottom). Scale bar: 50 μm. (**d, e**) A timeline demonstrating the subcutaneous injection of 1 × 10^7 WT cells and PACCs, followed by injection of DOX (2 mg/kg) into the tail vein (n = 6 per group) once a week when the tumor volume reached 150 mm^3. The photographs show representative tumors. (**f**) Animals were monitored for up to 36 days, and tumor size was measured using calipers at three-day intervals. (**g**) Representative images showing hematoxylin and eosin (H&E) staining (upper) or immunohistochemical staining for PCNA on paraffin sections of tumor tissues (bottom). Scale bar: 50 μm. (**h, i**) H&E staining was performed on a

triple negative breast cancer tissue microarray (TMA) with different tumor grades (grades 1, 2, 3, and negative) to detect PACCs. The number of PACCs was counted and analyzed from five randomly selected fields on each slide. The black boxes are magnified, and the orange arrows indicate PACCs. Scale bar: 500 μm. All data are presented as mean ± SEM; $*p < 0.05$, $**p < 0.01$, $***p < 0.001$; Student's two-tailed, unpaired t-test (a, b); one-way ANOVA with Bonferroni's post-test (**c, f, i**).

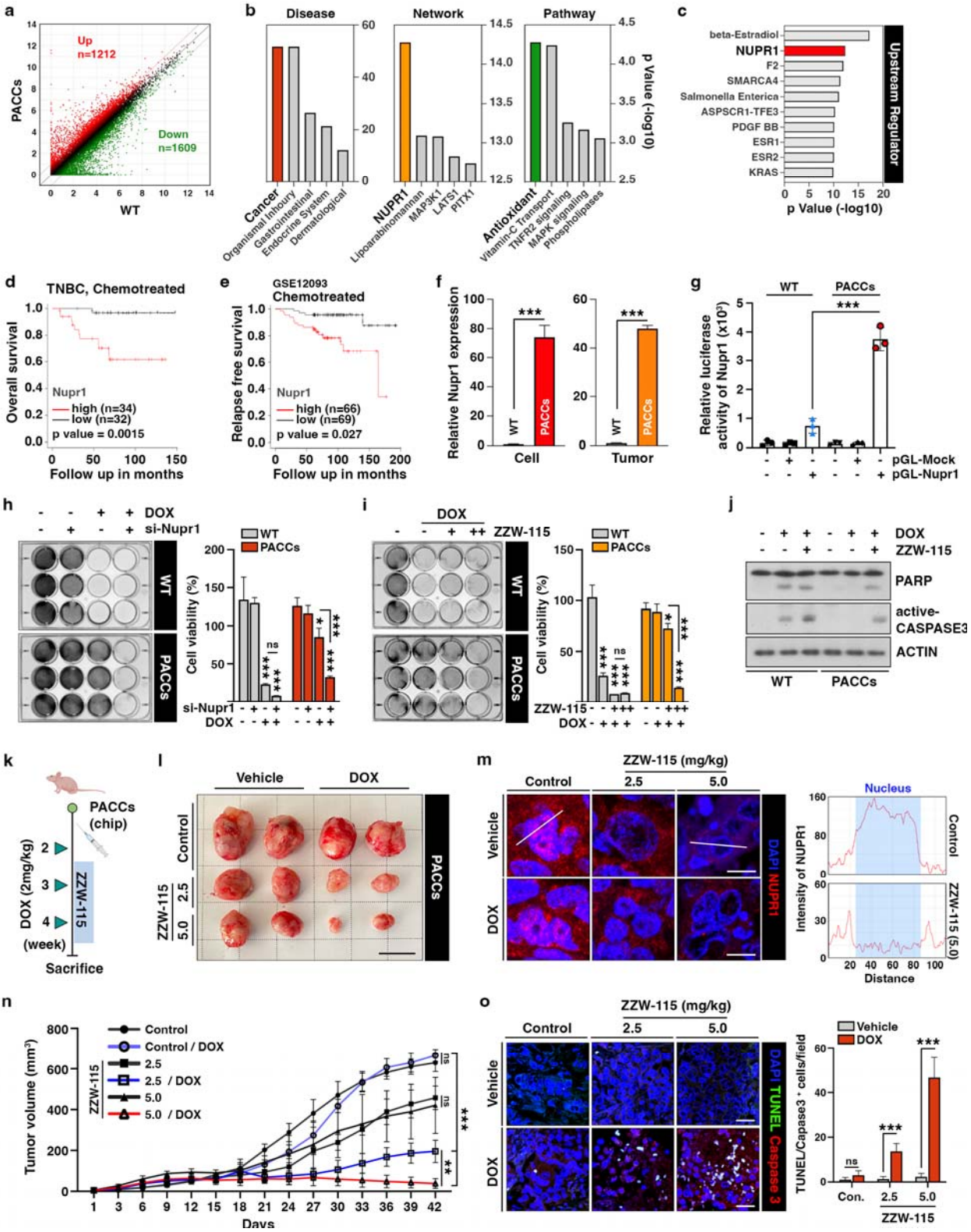

Fig. 4. Nupr1 is a key mediator of chemoresistance in PACCs. (**a**) Volcano plot of differential gene expression between WT cells and PACCs. Cut-off criteria included a fold change of 2. (**b, c**) Ingenuity Pathway Analysis (IPA) of the RNA-sequencing data shows disease and disorders (left), causal network (middle), canonical pathways (right), and upstream regulator (**c**). The top

five ranks are presented. Cut-off criteria are $p < 0.05$ and a false discovery rate (FDR) q-value < 0.05. (**d**) Kaplan-Meier (KM) survival curve represents the overall survival rate in chemotherapy-treated TNBC patients (n = 66) based on low vs. high Nupr1 expression from the meta-analysis in KM plotter. (**e**) KM survival curve representing the relapse-free survival rate in chemotherapy-treated patients (n = 135) based on low vs. high Nupr1 expression from GSE12093. (**f**) Reverse transcriptase-quantitative polymerase chain reaction (RT-qPCR) analysis of Nupr1 mRNA expression in cells (left) and tumor tissue from a mouse xenograft (right). The values were normalized to the level of the control (WT). (**g**) The relative luciferase activity of the Nupr1 promoter was measured in WT cells and PACCs. (**h**) Cell viability was measured among si-Nupr1 transfected cells treated with DOX using a crystal violet staining assay. (**i**) Cell viability was measured after administering DOX with and without ZZW-115 (Nupr1 inhibitor). The bar graph indicates the average density of dyed crystal violet. (**j**) Apoptotic proteins were detected by immunoblotting from WT cells and PACCs with and without DOX/ZZW-115. (**k**) Timeline demonstrating the subcutaneous injection of 1×10^7 PACCs followed by injections of doxorubicin (4 mg/kg) or ZZW-115 (2.5 mg/kg, 5.0 mg/kg) into the tail vein (n = 6 per group). (**l**) The photographs show representative tumors. Scale bar: 2 cm. (**m**) Representative images showing immunohistochemical staining for Nupr1 in PCGGs with and without ZZW-115 and DOX treatment (left). Localization of Nupr1 in the control and ZZW-115 (5.0 mg/kg)-injected tumors was analyzed by ImageJ (right). Scale bar: 20 μm. (**n**) Animals were monitored for up to 42 days, and tumor size was measured using calipers at three-day intervals. (**o**) Representative images showing immunohistochemical staining for TUNEL and active-caspase 3 on paraffin sections of tumor tissues. Scale bar: 20 μm. All data are presented as mean ± SEM; $^*p < 0.05$, $^{**}p < 0.01$, $^{***}p < 0.001$; Student's two-tailed, unpaired t-test (**f**); one-way ANOVA with Bonferroni's post-test (**g, h, i, n**).

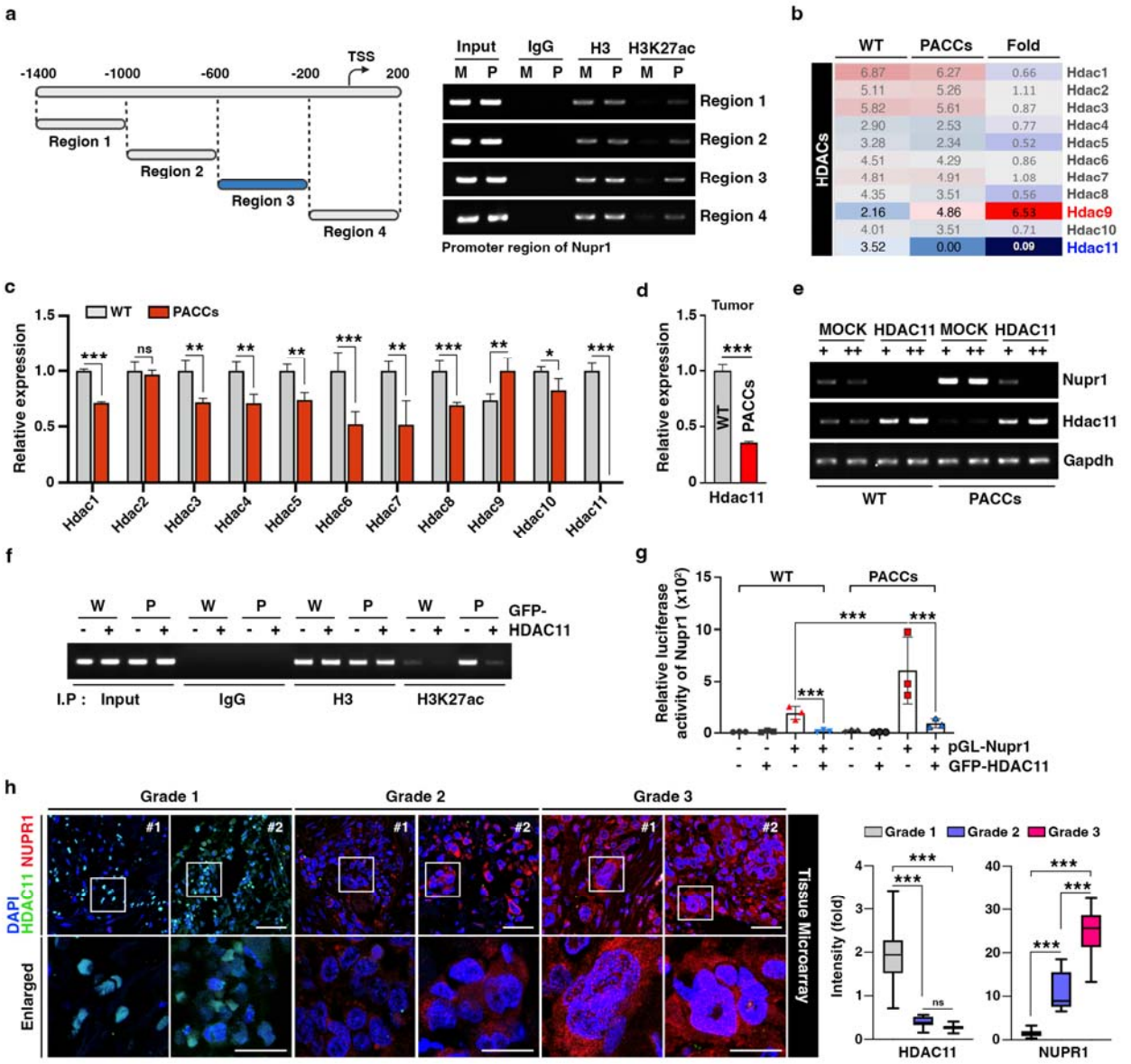

Fig. 5. HDAC11 suppression leads to Nupr1 upregulation in PACCs. (**a**) Schematic diagram showing the promoter region of Nupr1. A ChIP assay was performed with qPCR on WT cells and PACCs using anti-H3 and H3K27ac antibodies. W, WT; P, PACCs. (**b**) A heat map representing the relative mRNA expression levels of Hdacs in WT cells and PACCs. (**c**) Real-time PCR analysis of the mRNA expression of the indicated genes in WT cells and PACCs. (**d**) The mRNA expression of Hdac11 in PACC-derived tumor tissue was measured by RT-qPCR. (**e**) The mRNA expression of Nupr1 and Hdac11 was measured in cells transfected with either GFP-MOCK or HDAC11. (**f**) A ChIP assay was performed after transfecting WT and PACCs with GFP-MOCK or HDAC11 using anti-H3 or H3K27ac antibodies. Acetylated-histone levels were determined by RT-PCR with specific primers (-600/-200). W, WT; P, PACCs. (**g**) The relative luciferase activity of the Nupr1 promoter was measured after transfecting WT cells and PACCs with GFP-HDAC11. (**h**) Representative images show the expression of NUPR1 (red) and HDAC11 (green) on a TNBC

TMA with different tumor grades (grades 1, 2, and 3). Quantitative analysis of the intensity of NUPR1 and HDAC11 is displayed (right). White boxes are magnified. Scale bars: 50 μm (upper) and 25 μm (bottom). All data are presented as means ± SEM; $^{**}p < 0.01$, $^{***}p < 0.001$; Student's two-tailed, unpaired t-testing (**c, d**); one-way ANOVA with Bonferroni's post-test (**g, h**).

Supplementary Materials

Exploration of mechanisms of drug resistance by polyaneuploid cancer cells in a microfluidic device and patient tissues

Wanyoung Lim[1]†, Inwoo Hwang[2]†, Jiande Zhang[3], Zhenzhong Chen[3], Jeonghun Han[3], Bon-Kyoung Koo[4], Sangmin Kim[5], Jeong Eon Lee[6], Kenneth J. Pienta[7], Sarah R. Amend[7], Robert H. Austin[8], Jee-Yin Ahn[2,9,10]*, and Sungsu Park[1,3,11]*

[1]*Department of Biomedical Engineering, Sungkyunkwan University, Suwon 16419, South Korea*

[2]*Department of Molecular Cell Biology, Sungkyunkwan University School of Medicine, Suwon 16419, South Korea*

[3]*School of Mechanical Engineering, Sungkyunkwan University, Suwon 16419, South Korea*

[4]*Institute of Molecular Biotechnology of the Austrian Academy of Sciences (IMBA), Vienna Biocenter (VBC), 1030 Vienna, Austria*

[5]*Department of Breast Cancer Center, Samsung Medical Center, Sungkyunkwan University School of Medicine, Seoul 06351, South Korea*

[6]*Division of Breast Surgery, Department of Surgery, Samsung Medical Center, Sungkyunkwan University School of Medicine, Seoul 06351, South Korea*

[7]*The Cancer Ecology Center at the James Buchanan Brady Urological Institute, Johns Hopkins School of Medicine, Baltimore, MD 21205, USA*

[8]*Department of Physics, Princeton University, Princeton, NJ 08544, USA*

[9]*Single Cell Network Research Center, Sungkyunkwan University School of Medicine, Suwon 16419, South Korea*

[10]*Samsung Biomedical Research Institute, Samsung Medical Center, Sungkyunkwan University School of Medicine, Seoul 06351, South Korea*

[11]*Institute of Quantum Biophysics (IQB), Sungkyunkwan University, Suwon 16419, South Korea*

†These authors contributed equally to this work.

*Corresponding authors. E-mail: jeeahn@skku.edu; nanopark@skku.edu

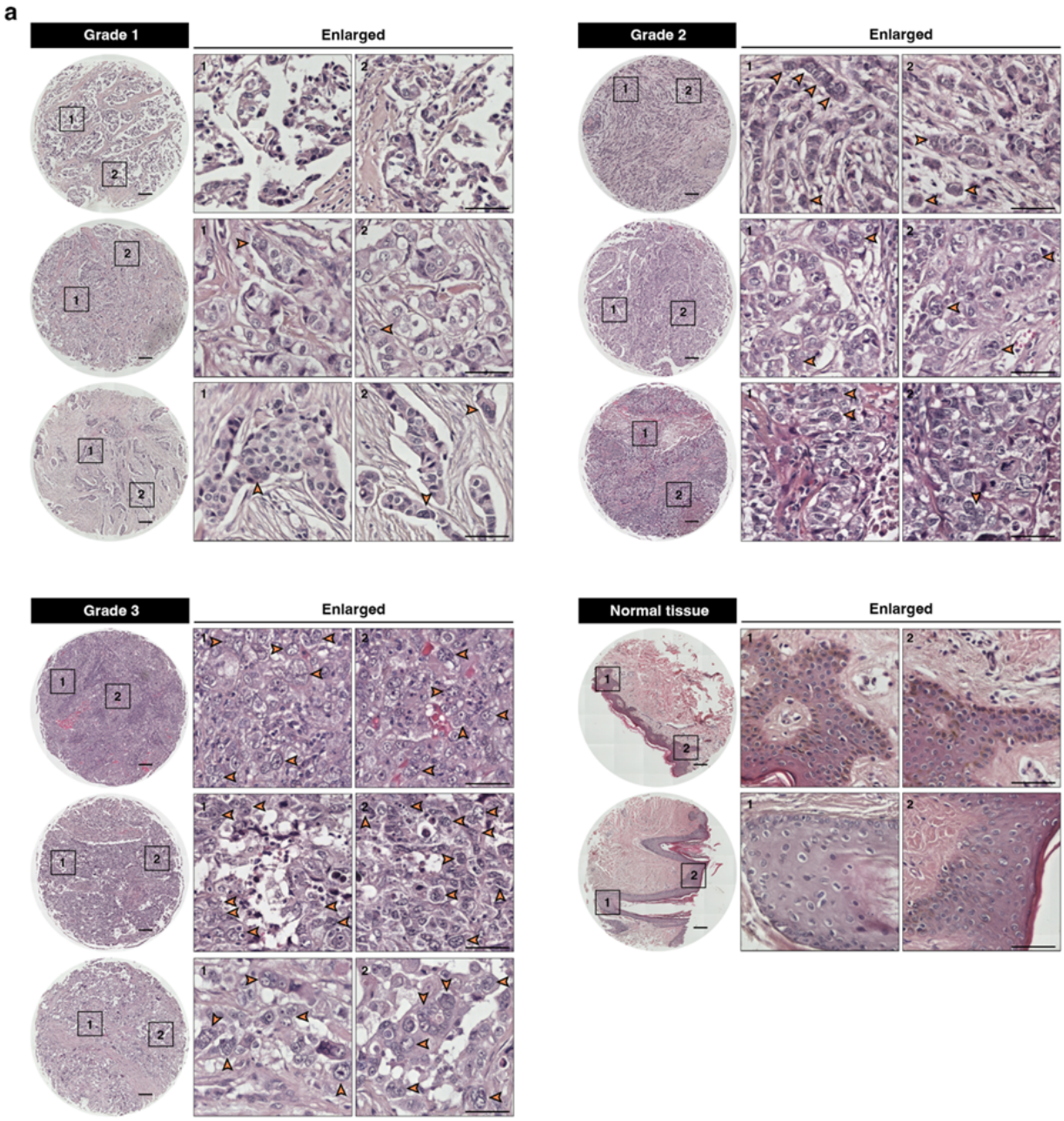

Fig. S1. Polyaneuploid cancer cells (PACCs) accelerate cancerous growth and tumor progression in triple negative breast cancer (TNBC). (**a**) Representative images showed TNBC tissue microarray (TMA, US Biomax #BR1301) with different tumor grades (grade 1, 2, 3, and negative) after stained with H&E (hematoxylin and eosin) for the detection of PACCs. Black boxes are magnified. Orange arrows indicate PACCs. Scale bar: 500 μm.

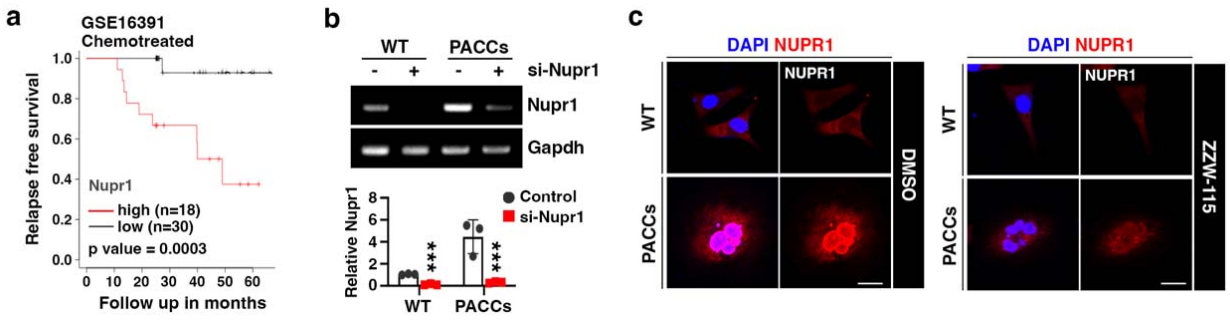

Fig. S2. Nupr1 is a key mediator of chemoresistance in PACCs. (**a**) Comparison of overall survival between high (red line) or low (blue line) expressions of Nupr1 in patients after chemo treated (GSE16391) were analyzed by the Kaplan-Meier (KM) and Log-rank test. KM survival curve representing the relapse-free survival rate in chemotherapy-treated patients (n=48) based on low (n=30) vs. high (n=18) Nupr1 expression. (**b**) si-Nupr1 was transfected into the wild type (WT) TNBC (MDA-MB-231) cells and PACCs and incubated for 24 h. The RNA expressions of Nupr1 were measured by RT-qPCR. (**c**) WT and PACCs were stained with anti-NUPR1 (red) after treated with ZZW-115. Scale bar: 20 μm. All data are presented as means ± SEM; ***p < 0.001; Student's two-tailed, unpaired t-test (b).

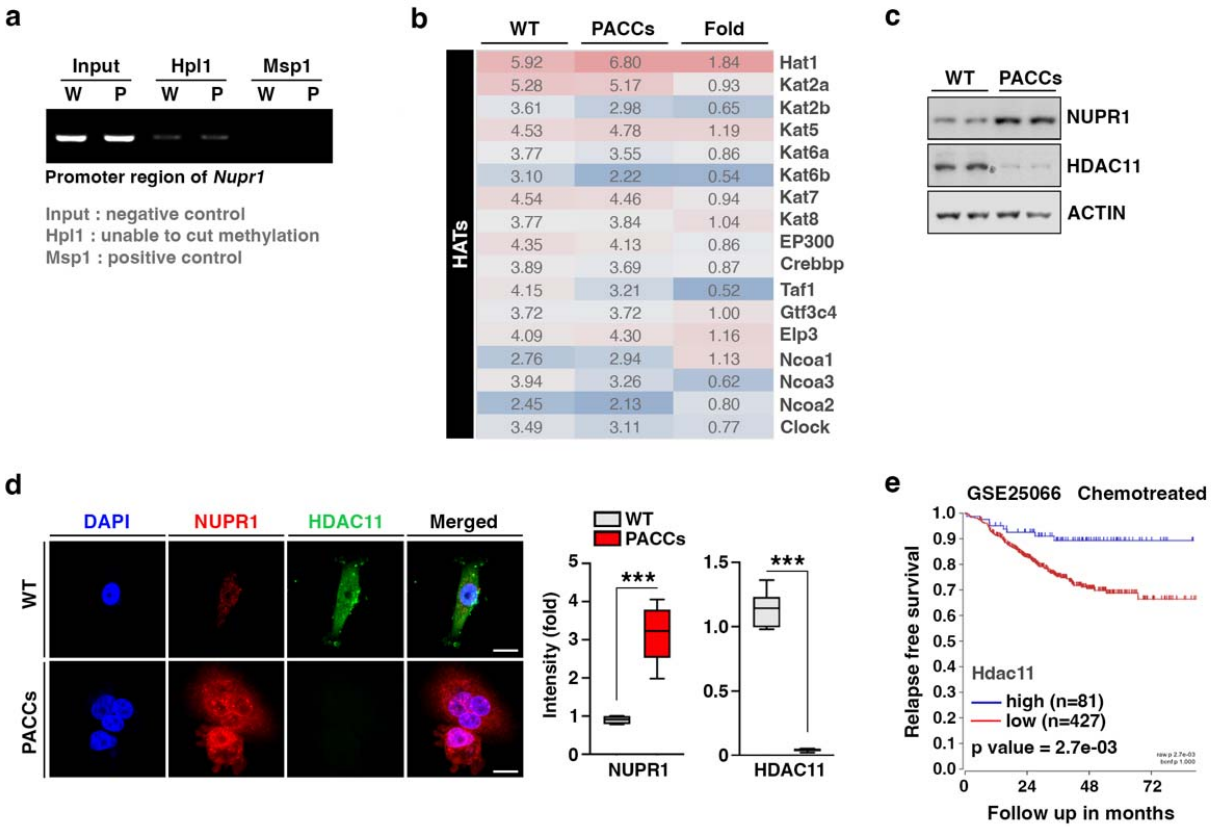

Fig. S3. HDAC11 suppression leads to Nupr1 upregulation in PACCs. (**a**) Extracted gDNA from WT and PACCs were digested with restriction enzymes that cut only non-methylated CCGG or cut all CCGG sequences. gDNA was assessed for methylation levels using qPCR with specific primer sets for CpG islands of Nupr1. W, WT; P, PACCs. (**b**) A heat map representing the relative mRNA expression levels of HDACs in WT or PACCs. (**c**) Protein expressions of NUPR1 and HDAC11 were measured from WT and PACCs by immunoblotting. (**d**) Cells were stained with anti-NUPR1 (red) and HDAC11 (green) antibodies for measuring their negative correlation. The intensity of NUPR1 and HDAC11 was measured by ImageJ. Scale bar: 20 μm. (**e**) Comparison of overall survival between high (n=81) or low (n=427) expressions of Hdac11 in patients after chemo treated (GSE25066, n=508) were analyzed by the Kaplan-Meier and Log-rank test. All data are presented as means ± SEM; ***$p < 0.001$; Student's two-tailed, unpaired *t*-test (**d**).

Table S1. List of primer sequences

ChIP assay primers		
Gene Name	**Forward Primer**	**Reverse Primer**
Nupr1 -1400/-1000	GATCTCAGCTCACCACAACCT	ATCTTCTTCCTAGAGTTGGGGAGA
Nupr1 -1000/-600	ACAATTATTATCATCCTTATTTTACAG	ATAGACATCTGCCACCATGCC
Nupr1 -600/-200	AATCCCAGCTATTCGGGAGG	ATATTTTCCATAGAGGAGGTCCCG
Nupr1 -200/+200	CCAGCTGGGTGAGCCTGG	AGATGGCTGAGTGGGCCTTA

Real-time qPCR primers		
Gene Name	**Forward Primer**	**Reverse Primer**
Gapdh	GTGTTCCTACCCCCAATGTGT	ATTGTCATACCAGGAAATGAGCTT
Nupr1	TCGGGCCTCTCATCATGCCT	TGCCCCTCGCTTCTTCCTCT
Hdac1	ATATCGGGGCTGGCAAAGGC	TCCACACACTTGGCGTGTCC
Hdac2	AGGCCCCATAAAGCCACTGC	CTCCAGCAACTGAACCGCCA
Hdac3	CTCAGCATCCGAGGGCATGG	TCGATGCGGGTGCTGACATC
Hdac4	GGTGGTGTTGGGGTGGACAG	GCTCTCCTCCGCATGGTGTC
Hdac5	CAACAGCTCCCACAGCACCA	TTGGTGACAGTGACCGTGGC
Hdac6	GACCTTGGAGCTAGGCAGCG	TGCCACCAAATGGGGACACC
Hdac7	CAGTGACCGCAGGACCCATC	CTGGGCAAAGTGGAAGGGCA
Hdac8	CAACACGGCTCGATGCTGGA	CGGCAGCTTGGCGTGATTTC
Hdac9	TATGGCACCAACCCCCTGGA	GCACCGGACGAGTGTAGCTC
Hdac10	CCTGGCCTATGGCTTCCAGC	TGCTAGCTGGGGTGTGGAGT
Hdac11	GTGCACACGAGGCGCTATCT	GCCAGCTTCCCCGCCATTAT